*Manuscript (including Abstract)
Click here to view linked References

https://doi.org/10.1016/j.electacta.2019.01.005

This is the Pre-Published Version.

Zeolitic imidazolate frameworks derived novel polyhedral shaped hollow Co-B-O@Co_3O_4 electrocatalyst for oxygen evolution reaction

Dongwon Kim[a,1], Daekyu Kim[a,1], Youngmoo Jeon[a], Yong Li[c], Jeongyeon Lee[a], Jeongmin Kang[a], Lawrence Yoon Suk Lee[c,*], Yuanzhe Piao[a,b,*]

[a] Department of Transdisciplinary Studies, Graduate School of Convergence Science and Technology, Seoul National University, Republic of Korea

[b] Advanced Institutes of Convergence Technology, Seoul National University, Suwon 16229, Republic of Korea

[c] Department of Applied Biology and Chemical Technology and the State Key Laboratory of Chirosciences, The Hong Kong Polytechnic University, Hung Hom, Kowloon, Hong Kong SAR, P. R. China

[1] These authors equally contributed to this work.

[*] Co-corresponding authors;

Yuanzhe Piao: Tel.: +82 31 888 9141; Fax: +82 31 888 9148; E-mail: parkat9@snu.ac.kr

Lawrence Yoon Suk Lee: Tel.: +852 3400 8696; Fax: +852 2364 9932; E-mail: lawrence.ys.lee@polyu.edu.hk

© 2019. This manuscript version is made available under the CC-BY-NC-ND 4.0 license https://creativecommons.org/licenses/by-nc-nd/4.0/.

Highlights

- Co-B-O@Co_3O_4 was prepared using calcination-$NaBH_4$ treatment strategy with a facile and energy efficient method.
- A distinctive polyhedral morphology of Co-B-O@Co_3O_4 was well preserved after the $NaBH_4$ treatment of its precursor material.
- Co-B-O@Co_3O_4 was employed for the electrochemical oxygen evolution reaction.
- Co-B-O@Co_3O_4 showed excellent catalytic performance and long-term durability for oxygen evolution reaction in basic media.

Abstract

The development of highly effective and low-cost non-noble metal electrochemical catalysts for oxygen evolution reactions (OER) is a major challenge for overall water splitting and rechargeable metal-air batteries. In this study, we develop a novel hollow cobalt-borate modified cobalt oxide composite (denoted by Co-B-O@Co_3O_4) catalyst derived from zeolitic imidazolate framework-67 (ZIF-67) for electrochemical OER. The Co-B-O@Co_3O_4 was easily synthesized via pyrolysis of ZIF-67 in Ar and air to produce hollow Co_3O_4 (denoted by h-Co_3O_4), followed by simple $NaBH_4$ treatment at ambient temperature for 4 hours. The unique polyhedral morphology was well preserved during the $NaBH_4$ treatment. Benefiting from its structural and compositional merit, the as-synthesized Co-B-O@Co_3O_4 exhibit excellent electrocatalytic activity and long-term stability for OER. Also, we conducted the OER test using a Co-B-O@Co_3O_4 catalyst in a neutral pH environment for further investigation. Our study can provide an insight into catalyst modification step to enhance the overall performance while keeping its physical structure simultaneously. using metal-organic framework for the electrochemical catalyst thus can be recognized as a method for producing a highly active, long-term working and novel engineered electrocatalyst for OER applications.

Keywords: Electrocatalyst, Oxygen evolution reaction, Metal-organic frameworks, ZIF-67, Cobalt boron composite

1. Introduction

The global demand for sustainable and clean energy for the next generation triggered the pursuit of finding promising electrocatalysts specialized in energy storage and conversion [1-4]. Among the energy conversion reactions, oxygen evolution reaction (OER) is a fundamental step in electrochemical water splitting and rechargeable metal-air batteries [5-8]. However, due to the sluggish kinetics of OER, the development of the suitable catalyst and devices has limited [9,10]. Because of the endergonic nature of the OER, a poor yield of oxygen generation and high energy consumption remain as a challenge. To achieve a high reaction rate, the catalyst must perform the OER at a low overpotential and the kinetics of the catalysis has to be facile. So far, some precious metal oxide materials such as RuO_2 and IrO_2 showed excellent performance as well as low overpotential toward OER process [11-14]. Nevertheless, these materials also possess some drawbacks like expensive cost, an insufficient amount of precursors and unsatisfying durability which slow down the large-scale industrial application. Also, RuO_2 and IrO_2 are known to dissolute in such high anodic potential, leading to the reduction of catalytic performance and stability [15]. On the other hand, various materials were investigated and evaluated to replace the precious metal oxide based catalyst [16-21]. Also, the optimization of size, morphology and electronic interaction is in progress by many scientists and engineers to accomplish the goal of making better electrocatalyst toward OER.

Among the possible alternative material to replace the precious metal-based catalyst, transition metal materials and derivatives can be attractive due to their well-known high performances, as well as their potential stability. From the Sabatier principle [22,23], cobalt-based materials showed the bright promise for OER electrocatalyst. Especially, cobalt-based

materials including hydroxides, oxyhydroxides, chalcogenides, phosphides and carbides [24-33] got its attention due to the excellent OER performance, strong stability and relatively low cost. However, the catalytic performance of these materials is still below their full capability. Also, a relatively high operating overpotential remains a challenge for practical applications.

Recently, cobalt-boron hybrid materials [34-36] got attention for its enhanced OER catalysis, along with easy and energy saving synthesis procedure. The introduction of boron species such as boride and borate into transition metal catalysts is known to aid the formation of metal oxyhydroxide (M-OOH) intermediates by decreasing the kinetic and thermodynamic barrier, which could eventually improve the performance of the electrochemical OER [37]. For a conventional application**,** the material is known for its ability to generate hydrogen from $NaBH_4$ by hydrolysis reaction [38,39]. Therefore, the material is under development as a catalyst in the field of reactor engineering for harvesting H_2 from the $NaBH_4$. The result showed that metal boron composite possesses the high ability to harvest hydrogen from $NaBH_4$ efficiently. Simagina et al. reported a cobalt boride catalyst for $NaBH_4$ hydrolysis using Co_3O_4 as a reacting material [40,41]. The mechanism suggests that Co_3O_4 initially become cobalt-boron composite when reacting with $NaBH_4$, then the subsequent hydrolysis of $NaBH_4$ is promoted by cobalt boride. Because of the catalytic effect of Co_3O_4 based cobalt-boron composite, the facile and moderate reaction rate could have achieved without influencing the catalytic performance. In the electrochemical perspective, Masa et al. reported easily synthesized amorphous cobalt boride for water splitting electrocatalyst [42]. The fabricated catalyst performed very well in an alkaline electrolyte and showed lower overpotential compared to the conventional precious metal oxide based electrocatalysts. Also, cobalt borate, due to their highly active catalytic ability on electrochemical OER, has been

reported recently [43-45]. Xue et al. reported that borate anion could influence the electronic structure of the cobalt-based electrocatalyst to generate a significant improvement in electrochemical OER activity [43]. However, the rapid and massive evolution of H_2 during the synthesis of the cobalt-boron composite is inevitable, thus remained as a challenge [46].

Zeolitic imidazolate frameworks (ZIFs), such as ZIF-67 and ZIF-8 are widely used metal-organic frameworks (MOFs) which possess uniform pore distribution and good chemical stability [47-49]. Due to these reasons, various electrocatalyst derived from ZIFs have been intensively investigated in recent years [50-56]. In many cases, ZIFs derived catalysts are prepared in high temperature or in the form of chalcogenide and phosphide with multiple preparation steps [57-62]. This process can further boost the performance and stability of the ZIFs derived catalyst.

Another great advantage of ZIFs derived catalyst is that the unique 3 D hollow and porous polyhedral morphology that can enhance the mass transfer efficiency [63-65], result in the improvement of the overall performance of the ZIFs derived catalysts. However, severe doping of heteroatoms and altering the physical-chemical structure of ZIFs can trigger the massive volume expansion within the material, which could damage the integrity of the material's structure and its structural merit [66-67]. Developing the ZIFs derived catalyst for the electrochemical OER by focusing the electrochemical performance is important. However, it is also crucial to develop the methodology for maintaining the structure during the preparation of ZIFs derived catalyst need to be proposed in order to keep the unique morphology and its structural advantage.

In viewing of these aforementioned perspectives in the electrochemical catalyst, we demonstrate ZIFs derived novel hollow cobalt borate modified cobalt oxide composite

(denoted by Co-B-O@Co_3O_4) catalyst for electrochemical OER. The Co-B-O@Co_3O_4 was easily synthesized via calcination-$NaBH_4$ treatment strategy. Initially, ZIF-67 was undergoing calcination process in Ar and air to produce hollow Co_3O_4 (denoted by h-Co_3O_4), followed by $NaBH_4$ treatment at ambient temperature for 4 h without further heat treatment. From the unusual calcination process of ZIF-67, the unique morphology and structure were well preserved with the fair amount of carbon which could help the catalyst's structural integrity [68]. Also, just adopting a simple $NaBH_4$ treatment step, turning h-Co_3O_4 into Co-B-O@Co_3O_4 was successful with the controlled material synthesis rate, well preserved physical structure and highly increased electrochemical OER performance compared to the h-Co_3O_4. After conducting OER test with prepared Co-B-O@Co_3O_4, the catalyst showed the overpotential of 0.350 V_{RHE} at 10 mA cm^{-2} with low Tafel slope of 32.7 mV dec^{-1} in 0.1 M KOH solution. Also, Co-B-O@Co_3O_4 performed at 0.343 V_{RHE} to reach 10 mA cm^{-2} with the Tafel slope of 40.3 mA dec^{-1} in 1.0 M KOH solution. Finally, the OER was performed under neutral pH condition for further investigation using Co-B-O@Co_3O_4.

2. Materials and methods

2.1 Reagents

All chemicals were used without further purification. Cobalt nitrate hexahydrate ($Co(NO_3)_2 \cdot 6H_2O$, 99.8%), methanol (99.8%), ethanol (99.9%), sodium borohydride ($NaBH_4$, 99.8%) and potassium hydroxide (KOH, 99.9%) were purchased from Samchun Chemicals (South Korea). 2-methylimidazole ($CH_3C_3H_2N_2H$, 99.0%) and Nafion solution (5 wt%) were purchased from Sigma-Aldrich (USA).

2.2 Apparatus

Electrochemical studies were conducted by using the conventional three-electrode system by an Autolab potentiostat (Metrohm, Netherlands). Glassy carbon electrode (GCE, 0.1963 cm^2 in surface area) was used as a working electrode. The Ag/AgCl with saturated KCl solution and Hg/HgO electrode with 1.0 M NaOH solution were used as reference electrodes. Platinum plate electrode (1.0 cm^2 in area) was used as a counter electrode. The produced materials were characterized by field-emission scanning electron microscope (FE-SEM, Hitachi S-4800). The energy-filtering transmission electron microscopy (EF-TEM) and the energy-dispersive X-ray spectroscopy (EDS) was also used (LIBRA 120). The electrochemical impedance spectroscopy (EIS, ZIVE SP1). The specific surface area and pore volume were analyzed via nitrogen adsorption-desorption isotherm (Micrometrics ASAP 2010). X-ray photoelectron spectroscopy (XPS) analysis was conducted using Axis-HIS spectrometer at a constant energy of 20 eV with Al irradiation of 12 kV and 18 mA. Inductively coupled plasma atomic emission spectroscopy (ICP-AES) analysis was conducted in Ar plasma (6000K) with the range of 167 – 782 nm (OPTIMA 8300, Perkin-Elmer). The thermogravimetric analysis (TGA) was performed using a TGA/DSC 1 analyzer (Mettler Toledo) with a ramp rate of 5 ℃ per minute in air.

2.3 Preparation of ZIF-67

Cobalt nitrate hexahydrate (1.165 g) and 2-methylimidazole (1.315 g) were dissolved in methanol (100ml) separately. The above two solutions were then mixed for 5 minutes. The

resulting solution was aged at room temperature for 24 h. Then the resulting purple precipitate was washed with ethanol for three times and collected by centrifugation. Finally, the product was dried in an oven at 60 ℃ for 12 h.

2.4 Preparation of h-Co_3O_4

The prepared ZIF-67 (0.1 g) was heated at 350 ℃ with a rate of 5 ℃/min using horizontal quartz furnace tube and maintained at this temperature for 30 min under Ar environment. Then, the Ar gas was switched to air and kept at the same temperature for another 30 min. Prepared h-Co_3O_4 was then washed with H_2O and dried in an oven at 60 ℃ for 12 h.

2.5 Preparation of Co-B-O@Co_3O_4

The as-obtained h-Co_3O_4 (0.03 g) was dispersed in 15 ml of H_2O and maintained at 5 ℃ using an ice-bath for 20 min. $NaBH_4$ (0.1893 g) was dissolved in 5 ml H_2O and added to the above solution by syringe with vigorous stirring for 4 hours. After the $NaBH_4$ treatment, the resulting precipitate was centrifuged and washed with water several times and dried at 60 ℃ oven for 12 h and denoted by Co-B-O@Co_3O_4. For the comparison, the samples were prepared according to the various $NaBH_4$ treatment time (2, 6 and 8h) and denoted by Co-B-O@Co_3O_4-2h, Co-B-O@Co_3O_4-6h and Co-B-O@Co_3O_4-8h, respectively.

2.6 Electrochemical measurements

To conduct the electrochemical measurements, the catalyst inks were prepared in following steps. Initially, the prepared catalyst (4.95 mg) was dispersed in a mixture of ethanol (0.75

mL) and water (0.20 mL). Subsequently, Nafion solution (5 wt%, 0.02 mL) was added to the above mixture, followed by ultrasonication for 30 min to produce a well-dispersed solution. In the process of electrode fabrication, 0.01 mL of the prepared ink was dropped on an alumina polished GCE (calculated amount of material loading was 0.255 mg cm^{-2}) and dried under an infrared lamp for 10 min. For the electrochemical stability test, the electrode was fabricated using Ni foam (1 cm^2 in area).

All measured potentials were converted to the reversible hydrogen electrode (RHE) scale from Ag/AgCl and Hg/HgO reference electrodes according to the equation;

$E_{RHE} = E_{Ag/AgCl} + 0.059pH + 0.1976$, $E_{RHE} = E_{Hg/HgO} + 0.059pH + 0.140$

It should be noted that any indication regarding the potentials is referred to RHE in 0.1 M and 1.0 M KOH solution without specification. The OER measurements were investigated in KOH electrolyte with a predetermined concentration. The rotation speed of the rotating disk electrode (RDE) was 1600 rpm for all measurements. Before acquiring any electrochemical data, the electrolytes were purged with O_2 for 30 min. Prior to the linear sweep voltammetry (LSV) test, a conditioning step was applied by continuous cyclic voltammetry (CV) for 15 times between 0.96 and 1.76 V with a scan rate of 0.1 V s^{-1}. The LSV curves were measured from 0.96 to 1.96 V with a scan rate of 5 mV s^{-1} in KOH (0.1 and 1.0 M). The long-term performance of the catalysts was evaluated with chronoamperometry in KOH (0.1 and 1.0 M) solution to maintain the current density of 10 mA cm^{-2}. All the data were corrected for the iR_S compensation. The EIS measurements were carried out in the frequency range from 10^{-1} to 10^5 Hz at 1.47 V. The electrochemical double layer capacitance (C_{dl}) of different catalysts were measured by using cyclic voltammetry in a non-faradaic region (1.20 – 1.40 V) at series of scan rates of 20, 40, 60, 80, 100, 120, 140, 160, 180 and 200 mV s^{-1}.

3. Result and discussion

The schematic illustration for the fabrication of the Co-B-O@Co_3O_4 is shown in Scheme 1. In brief, the h-Co_3O_4 was synthesized from the ZIF-67 by two-step thermal conversion process under argon and air at 350 ℃ respectively. Then, the Co-B-O@Co_3O_4 was obtained through the $NaBH_4$ treatment process of h-Co_3O_4 under the action of the $NaBH_4$ at ambient temperature for 4 h.

The size and morphology of the as-synthesized materials were initially investigated by SEM. As shown in Fig. S1(in the supplementary information, SI), the as-synthesized ZIF-67 shows smooth polyhedral morphology and have good uniformity with the well-distributed size of 1.0 μm in width. Fig. 1 shows the SEM image of the h-Co_3O_4 and Co-B-O@Co_3O_4. In the case of h-Co_3O_4 (Fig. 1a, b), the illustration demonstrates that the polyhedral morphology of ZIF-67 is quite well preserved but become slightly rough on the surface. In the case of Co-B-O@Co_3O_4 (Fig. 1c, d), the surface of the material becomes rougher than h-Co_3O_4, but hollow polyhedral morphology was well maintained. Also, overall size and physical structure of the Co-B-O@Co_3O_4 was not drastically changed compared to the h-Co_3O_4. This result indicates that the $NaBH_4$ treatment did not severely modify the polyhedral morphology of the h-Co_3O_4.

The morphology and interior structure of the Co-B-O@Co_3O_4 was further elucidated by TEM (Fig. 2). The dodecahedron-like shell structures can be observed more distinctly and the hollow interiors are clearly revealed by the sharp contrast between the centers and edges of the Co-B-O@Co_3O_4 from the TEM image in Fig. 2a. It is noticeable that the polyhedral morphology of Co-B-O@Co_3O_4 was well preserved due to the fact that carbon generated at the first calcination act as a temporal structure buffer, which helps to preserve the

morphology of ZIF-67. As observed by SEM and TEM data, we speculate that the physical structure of the h-Co_3O_4 and Co-B-O@Co_3O_4 are not been altered greatly. The EDS mapping (Fig. 2b – e) was employed to determine the elemental distribution of Co-B-O@Co_3O_4, which show the co-existence and the uniform distribution of Co, O and B on the prepared catalyst.

To investigate the amount of Co and B, an ICP-AES study have been explored. The investigation revealed that the product in consisted of mainly Co (67.17 wt%) and a small amount of B (0.10 wt%), the rest being C and O. The corresponding atomic ratio between Co and B was 1.0:0.08.

More detail characterization of Co-B-O@Co_3O_4 was conducted with XPS measurement (Fig. 3). The high-resolution spectrum indicates the separation of Co 2p peak with $2p_{3/2}$ and $2p_{1/2}$ components due to the spin-orbit splitting, accompanied by two satellite peaks (Fig. 3a). The binding energy of the main Co $2p_{3/2}$ and $2p_{1/2}$ peak was 780.7 and 796.5 eV, respectively, indicating the typical representation of $Co(OH)_2$ which was inadvertently formed by $NaBH_4$ treatment and exposure to air [69]. The binding energy of the main O 1s peak was 531.4 eV, which is a contribution of four different peaks (Fig. 3b) [69]. Mainly, the peak is associated with metal hydroxide species (531.2 eV), which can be interpreted as the possible formation of $Co(OH)_2$ during the $NaBH_4$ treatment. Other peaks indicate the presence of metal oxides (529.8 eV), the mixed peak of adsorbed water and C-O species (532.2 eV) and C=O species (533.3 eV). The B 1s spectrum of Co-B-O@Co_3O_4 was represented into a distinctive peak at 191.8 eV (Fig. 3c). The peak is assigned to the boron-oxo species such as cobalt borate [42]. From the designated XPS data, it is plausible to speculate that the simultaneous formulation of cobalt borate composite was produced during the $NaBH_4$ treatment process. The atomic

percentage of Co, B and O calculated from the XPS data was 15.3 %, 7.9 % and 43.9 %, respectively. Combining this result with the ICP-AES data, we speculate the majority of the B related species such as cobalt borate composite exists on the surface of the material. Therefore, it is possible to consider that only a slight alteration of the catalyst's exterior was happened during the $NaBH_4$ treatment of h-Co_3O_4 to produce Co-B-O@Co_3O_4.

The TGA was performed to calculate the weight percentage of C in the Co-B-O@Co_3O_4 (Fig. S2 in the SI). The investigation suggests that the Co-B-O@Co_3O_4 contains 8.9 wt% of C. Judging by the degradation curve [70], we speculate that the retained C in the Co-B-O@Co_3O_4 mostly exists as the form of carbonate. Also, judging by the scarce amount of retained carbon in Co-B-O@Co_3O_4, it is possible to consider that the carbon acted as a binder to keep the polyhedral structure during the calcination process.

The BET surface area, total pore volume and mean pore diameter of the h-Co_3O_4 and Co-B-O@Co_3O_4 was investigated through N_2 adsorption-desorption hysteresis (Fig. 3d) The hysteresis diagram and pore distribution diagram of h-Co_3O_4 and Co-B-O@Co_3O_4 showed a high degree of resemblance with little contrast. According to the SEM data and the N_2 adsorption-desorption hysteresis result, we assume that the surface of Co-B-O@Co_3O_4 has not been severely enlarged or etched away during the $NaBH_4$ treatment. The result indicates that the surface morphology has not been altered greatly, thus can be a supporting evidence for the physical stability of the material that undergone $NaBH_4$ treatment. Summarized information of the BET surface area, total pore volume and mean pore diameter are presented in Table 1.

Table 1. The BET surface area, pore volume and mean pore diameter of h-Co_3O_4 and Co-O-B@Co_3O_4

	h-Co_3O_4	Co-O-B@Co_3O_4

BET surface area (m^2 g^{-1})	49.26	55.08
Total pore volume (cm^3 g^{-1})	0.33	0.35
Mean pore diameter (nm)	26.70	25.33

The examination of electrochemical OER demeanor of the Co-B-O@Co_3O_4 was investigated in 0.1 M KOH solution. For the comparison, prepared RuO_2, h-Co_3O_4, Co-B-O@Co_3O_4-2h, Co-B-O@Co_3O_4-6h and Co-B-O@Co_3O_4-8h were also investigated in the same experimental condition. Fig. 4a shows iR_S corrected LSV of OER using prepared modified electrodes. The result indicates that among the materials, Co-B-O@Co_3O_4 shows the small onset potential of 1.47 V for the OER, beyond which oxidation current rises rapidly by applying a little overpotential (from 5.00 mA cm^{-2} at 1.50 V and 20.90 mA cm^{-2} at 1.56 V). Also, from the linear regions of the Tafel plots (Fig. 4b), the Tafel slope was calculated [71]. From the equation, the high catalytic activity of the Co-B-O@Co_3O_4 is described by its Tafel slope of 32.7 mA dec^{-1}. Other compared materials such as h-Co_3O_4 (72.4 mA dec^{-1}), Co-B-O@Co_3O_4-2h (54.3 mA dec^{-1}), Co-B-O@Co_3O_4-6h (63.5 mA dec^{-1}) and Co-B-O@Co_3O_4-8h (57.9 mA dec^{-1}) showed inferior results. This result demonstrates that the Co-B-O@Co_3O_4 is remarkably more active toward OER. The onset potential and Tafel slope of RuO_2 is 1.37 V and 68.8 mA dec^{-1}, respectively. Although the onset potential of Co-B-O@Co_3O_4 is higher than RuO_2, the result from the Tafel slope indicates that the Co-B-O@Co_3O_4 has a greater advantage in OER kinetics. Achieving 10 mA cm^{-2} at low overpotential is another criterion for evaluating materials for OER catalyst. In the case of Co-B-O@Co_3O_4, the measured overpotential was 0.350 V to reach 10 mA cm^{-2}, indicating an excessive performance for OER. Compared to this result, other materials such as h-Co_3O_4 (0.495 V), Co-B-O@Co_3O_4-2h (0.393 V), Co-B-O@Co_3O_4-6h (0.402 V) and Co-B-O@Co_3O_4-8h (0.387 V) showed

higher overpotential to reach 10 mA cm^{-2}. The stability of the Co-B-O@CO_3O_4 was measured with chronoamperometry in 0.1 M KOH solution for 12 h to maintain the current density of 10 mA cm^{-2} (Fig. 4c). Even though the result showed a weak decay of catalytic performance, the catalyst could operate for 12 h and as much as 70 % of its original catalytic capability was still maintained.

To further study on the electrocatalytic activity of the as-synthesized materials, the electrochemical performance testing of the as-prepared materials were also investigated in 1.0 M KOH solution. Fig. 4d shows the LSV curves of prepared RuO_2, h-Co_3O_4, Co-B-O@Co_3O_4, Co-B-O@Co_3O_4-2h, Co-B-O@Co_3O_4-6h and Co-B-O@Co_3O_4-8h catalysts with iR_S correction in 1.0 M KOH. The result indicates that among the materials except for RuO_2, Co-B-O@Co_3O_4 exhibits the lowest onset potential at 1.47 V for OER, which the current density rapidly rises with the small increase of overpotential (from 20.00 mA cm^{-2} at 1.584 V and 80.00 mA cm^{-2} at 1.597 V). The result of the calculated Tafel slope of Co-B-O@Co_3O_4 was 40.3 mA dec^{-1} (Fig. 4e). The other compared catalysts like h-Co_3O_4 (74.6 mA dec^{-1}), Co-B-O@Co_3O_4-2h (64.6 mA dec^{-1}), Co-B-O@Co_3O_4-6h (62.3 mA dec^{-1}) and Co-B-O@Co_3O_4-8h (45.6 mA dec^{-1}) showed higher Tafel slope value, indicating the inferior OER kinetics. The required overpotential for Co-B-O@Co_3O_4 to reach 10 mA cm^{-2} was 0.343 V. Other compared catalysts such as h-Co_3O_4 (0.411 V), Co-B-O@Co_3O_4-2h (0.367 V), Co-B-O@Co_3O_4-6h (0.352 V) and Co-B-O@Co_3O_4-8h (0.355 V) required higher overpotential to reach the current density of 10 mA cm^{-2}. The overpotential at 10 mA cm^{-2} of RuO_2 is 0.233 V. The value of Tafel slope of Co-B-O@Co_3O_4 was still low even compared to the RuO_2 (43.1 mA dec^{-1}), implying that the Co-B-O@Co_3O_4 has favorable OER kinetics. To investigate the durability of the Co-B-O@Co_3O_4 under 1.0 M KOH, 12 h of chronoamperometry to maintain

the 10 mA cm^{-2} was implied (Fig. 4f). The Co-B-O@Co_3O_4 catalyst performed well with the small reduction of catalytic capability and the current density was persisted for 12 h. In addition, we demonstrated the OER at pH=7.4 environment using 1.0 M phosphate buffer solution (PBS) (Fig. S4 in SI). The overall electrochemical results are summarized in Table S1. in SI. Compared with several other reported catalysts (Table S4. and Table S5. in the SI), the prepared Co-B-O@Co_3O_4 performed well considering the simple and easy preparation process.

The Nyquist plots demonstrate that Co-B-O@Co_3O_4 showed the smallest semicircle diameter than other compared materials in both 0.1 M and 1.0 M KOH, respectively (Fig. S3). This result suggests a lower charge transfer resistance (R_{ct}) of Co-B-O@Co_3O_4, therefore better catalytic activity of the material is reasonable. From the equivalent electrical circuit, the R_{ct} of Co-B-O@Co_3O_4 was calculated as 8.069 Ω. In the case of other prepared catalysts, the R_{ct} value was high than Co-B-O@Co_3O_4 except for RuO_2. Further information is represented in Table S2. in SI. The electrochemical active surface area of the catalysts was examined from the double-layer capacitance (C_{dl}), which was calculated by CV in non-faradic potential range with various scan rates from 20 to 200 mV s^{-1} (Fig. 5a - e). From the CV, the linear plot (Fig. 5f) of scan rate versus current density and the calculated value of C_{dl} were obtained. The C_{dl} of h-Co_3O_4 was the lowest of 1.33 mF cm^{-2}, followed by Co-B-O@Co_3O_4-6h (4.44 mF cm^{-2}), Co-B-O@Co_3O_4-2h (8.36 mF cm^{-2}) and Co-B-O@Co_3O_4-8h (17.03 mF cm^{-2}). The Co-B-O@Co_3O_4 showed the highest C_{dl} value of 26.20 mF cm^{-2}, which can be an indication that the material has the largest electrochemical active surface area. The summarized result of the C_{dl} calculation is presented in Table S3. in SI.

4. Conclusion

In summary, we designed and produced a novel Co-B-O@Co_3O_4 catalyst through a calcination-$NaBH_4$ treatment strategy using ZIF-67 as a source material. Initially, during the production process of h-Co_3O_4 using Ar and air from ZIF-67, the certain degree of carbon was remained and enforced the structural integrity of the h-Co_3O_4. Subsequently, the material was treated with an aqueous solution of $NaBH_4$ for 4 h to fabricate Co-B-O@Co_3O_4 catalyst from h-Co_3O_4. By introducing a simple modification step, the efficiency of Co-B-O@Co_3O_4 toward OER was greatly increased. Also, the unique polyhedral morphology of the precursor material was still intact during the $NaBH_4$ treatment. This result indicates the mild degree of alteration of precursor material and was fully able to exploit the structural advantage. Novel Co-B-O@Co_3O_4 catalyst exhibited excellent performance toward electrochemical OER compared to h-Co_3O_4. In the case of 0.1 M and 1.0 M KOH, Co-B-O@Co_3O_4 needed the overpotential of 0.350 V and 0.342 V respectively to reach 10 mA cm^{-2}. To determine the stability of the Co-B-O@Co_3O_4, the continuous 12 h chronoamperometry tests under 0.1 M and 1.0 M KOH were also initiated. The catalyst performed well in both alkaline condition with little decay of catalytic ability. Because of the complex nature of the catalyst's component, it is difficult to investigate the exact quality and quantity of elements constructing the Co-B-O@Co_3O_4. Nevertheless, this work can suggest a new insight into the development of novel structured catalyst not only by its performance but also the structural merit. Also, by achieving low energy consumption during the fabrication of catalyst, this work can be acknowledged as a new approach toward energy saving methods for future electrocatalyst development and its energy conversion applications.

Acknowledgments

This research was supported by the Basic Science Research Program through the National Research Foundation of Korea (NRF) funded by the Ministry of Education (NRF-2018R1D1A1B07051249) and Nano Material Technology Development Program (NRF-2015M3A7B6027970) of MSIP/NRF. This research was also supported by the Center for Integrated Smart Sensors funded by the Ministry of Science, ICT and Future Planning, Republic of Korea, as Global Frontier Project (CISS-2012M3A6A6054186).

References

[1] M. Tahir, L. Pan, F. Idrees, X. Zhang, L. Wang, J.J. Zou, Z.L. Wang, Electrocatalytic oxygen evolution reaction for energy conversion and storage: A comprehensive review, Nano Energy. 37 (2017) 136.

[2] X. Liu, L. Dai, Carbon-based metal-free catalysts, Nat. Rev. Mater. 1 (2016) 16064.

[3] M. Gong, H. Dai, A mini review of NiFe-based materials as highly active oxygen evolution reaction electrocatalysts, Nano Res. 8 (2015) 23.

[4] D.U. Lee, P. Xu, Z.P. Cano, A.G. Kashkooli, M.G. Park, Z. Chen, Recent progress and perspectives on bi-functional oxygen electrocatalysts for advanced rechargeable metal-air batteries, J. Mater. Chem. A. 4 (2016) 7107.

[5] H. Wang, H.W. Lee, Y. Deng, Z. Lu, P.C. Hsu, Y. Liu, D. Lin, Y. Cui, Bifunctional non-noble metal oxide nanoparticle electrocatalysts through lithium-induced conversion for overall water splitting, Nat. Commun. 6 (2015) 7261.

[6] M.I. Jamesh, Recent progress on earth abundant hydrogen evolution reaction and oxygen evolution reaction bifunctional electrocatalyst for overall water splitting in alkaline media, J. Power Sources. 333 (2016) 213.

[7] Z.L. Wang, D. Xu, J.J. Xu, X.B. Zhang, Oxygen electrocatalysts in metal-air batteries: From aqueous to nonaqueous electrolytes, Chem. Soc. Rev. 43 (2014) 7746.

[8] G. Li, X. Wang, J. Fu, J. Li, M.G. Park, Y. Zhang, G. Lui, Z. Chen, Pomegranate-Inspired Design of Highly Active and Durable Bifunctional Electrocatalysts for Rechargeable Metal-Air Batteries, Angew. Chem. Int. Ed. 55 (2016) 4977.

[9] W.T. Hong, M. Risch, K.A. Stoerzinger, A. Grimaud, J. Suntivich, Y. Shao-Horn, Toward the rational design of non-precious transition metal oxides for oxygen electrocatalysis, Energy Environ. Sci. 8 (2015) 1404.

[10] F. Song, X. Hu, Exfoliation of layered double hydroxides for enhanced oxygen evolution catalysis, Nat. Commun. 5 (2014) 4477.

[11] C.C.L. McCrory, S. Jung, J.C. Peters, T.F. Jaramillo, Benchmarking Heterogeneous Electrocatalysts for the Oxygen Evolution Reaction, J. Am. Chem. Soc. 135 (2013) 16977.

[12] Y. Lee, J. Suntivich, K.J. May, E.E. Perry, Y. Shao-Horn, Synthesis and Activities of Rutile IrO_2 and RuO_2 Nanoparticles for Oxygen Evolution in Acid and Alkaline Solutions, J. Phys. Chem. Lett. 3 (2012) 399.

[13] Z. Jian, P. Liu, F. Li, P. He, X. Guo, M. Chen, H. Zhou, Core-Shell-Structured CNT@RuO_2 Composite as a High-Performance Cathode Catalyst for Rechargeable Li-O_2 Batteries, Angew. Chem. Int. Ed. 53 (2014) 442.

[14] J. Lim, D. Park, S.S. Jeon, C.W. Roh, J. Choi, D. Yoon, M. Park, H. Jung, H. Lee, Ultrathin IrO_2 Nanoneedles for Electrochemical Water Oxidation, Adv. Funct. Mater. 28 (2018) 1704796.

[15] S. Cherevko, S. Geiger, O. Kasian, N. Kulyk, J.-P. Grote, A. Savan, B.R. Shrestha, S. Merzlikin, B. Breitbach, A. Ludwig, K.J.J. Mayrhofer, Oxygen and hydrogen evolution reactions on Ru, RuO_2 , Ir, and IrO_2 thin film electrodes in acidic and alkaline electrolytes: A comparative study on activity and stability, Catal. Today. 262 (2016) 170.

[16] Z. Lu, H. Wang, D. Kong, K. Yan, P.C. Hsu, G. Zheng, H. Yao, Z. Liang, X. Sun, Y. Cui, Electrochemical tuning of layered lithium transition metal oxides for improvement of oxygen evolution reaction, Nat. Commun. 5 (2014) 4345.

[17] Y. Wang, J. Li, Z. Wei, Transition-metal-oxide-based catalysts for the oxygen reduction reaction, J. Mater. Chem. A. 6 (2018) 8194.

[18] Y. Huang, C. Feng, H. Wu, S. Wang, F. Wang, H. Liu, Hybrids of Fe_3O_4oSe_2 as efficient electrocatalysts for oxygen reduction reaction, J. Mater. Sci. 53 (2018) 1123.

[19] F. Song, L. Bai, A. Moysiadou, S. Lee, C. Hu, L. Liardet, X. Hu, Transition Metal Oxides as Electrocatalysts for the Oxygen Evolution Reaction in Alkaline solutions: An Application-Inspired Renaissance, J. Am. Chem. Soc. 140 (2018) 7748.

[20] W. Xu, F. Lyu, Y. Bai, A. Gao, J. Feng, Z. Cai, Y. Yin, Porous cobalt oxide nanoplates enriched with oxygen vacancies for oxygen evolution reaction, Nano Energy. 43 (2018) 110.

[21] J. Fang, L. Hu, M. Wang, L. Gan, C. Chen, Y. Jiang, B. Xiao, Y. Lai, J. Li, NiO-Fe_2O_3/carbon nanotubes composite as bifunctional electrocatalyst for rechargeable Zn-air batteries, Mater. Lett. 218 (2018) 36.

[22] A.J. Medford, A. Vojvodic, J.S. Hummelshøj, J. Voss, F. Abild-Pedersen, F. Studt, T. Bligaard, A. Nilsson, J.K. Nørskov, From the Sabatier principle to a predictive theory of transition-metal heterogeneous catalysis, J. Catal. 328 (2015) 36.

[23] E. Fabbri, A. Habereder, K. Waltar, R. Kötz, T.J. Schmidt, Developments and perspectives of oxide-based catalysts for the oxygen evolution reaction, Catal. Sci. Technol. 4 (2014) 3800.

[24] J. Liu, J. Nai, T. You, P. An, J. Zhang, G. Ma, X. Niu, C. Liang, S. Yang, L. Guo, The Flexibility of an Amorphous Cobalt Hydroxide Nanomaterial Promotes the Electrocatalysis of Oxygen Evolution Reaction, Small. 14 (2018) 1703514.

[25] S. Feng, C. Liu, Z. Chai, Q. Li, D. Xu, Cobalt-based hydroxide nanoparticles@N-doping carbonic frameworks core–shell structures as highly efficient bifunctional electrocatalysts for oxygen evolution and oxygen reduction reactions, Nano Res. 11 (2018) 1482.

[26] Z. Chen, C.X. Kronawitter, Y.W. Yeh, X. Yang, P. Zhao, N. Yao, B.E. Koel, Activity of pure and transition metal-modified CoOOH for the oxygen evolution reaction in an alkaline medium, J. Mater. Chem. A. 5 (2017) 842.

[27] R. Takeuchi, T. Sato, K. Tanaka, K. Aiso, D. Chandra, K. Saito, T. Yui, M. Yagi, Superior Inorganic Ion Cofactors of Tetraborate Species Attaining Highly Efficient Heterogeneous Electrocatalysis for Water Oxidation on Cobalt Oxyhydroxide

Nanoparticles, ACS Appl. Mater. Interfaces. 9 (2017) 36955.

[28] X. Ma, W. Zhang, Y. Deng, C. Zhong, W. Hu, X. Han, Phase and composition controlled synthesis of cobalt sulfide hollow nanospheres for electrocatalytic water splitting, Nanoscale. 10 (2018) 4816.

[29] W. Li, X. Gao, D. Xiong, F. Wei, W.G. Song, J. Xu, L. Liu, Hydrothermal Synthesis of Monolithic Co_3Se_4 Nanowire Electrodes for Oxygen Evolution and Overall Water Splitting with High Efficiency and Extraordinary Catalytic Stability, Adv. Energy Mater. 7 (2017) 1602579.

[30] C.Z. Yuan, S.L. Zhong, Y.F. Jiang, Z.K. Yang, Z.W. Zhao, S.J. Zhao, N. Jiang, A.W. Xu, Direct growth of cobalt-rich cobalt phosphide catalysts on cobalt foil: an efficient and self-supported bifunctional electrode for overall water splitting in alkaline media, J. Mater. Chem. A. 5 (2017) 10561.

[31] H. Li, Q. Li, P. Wen, T.B. Williams, S. Adhikari, C. Dun, C. Lu, D. Itanze, L. Jiang, D.L. Carroll, G.L. Donati, P.M. Lundin, Y. Qiu, S.M. Geyer, Colloidal Cobalt Phosphide Nanocrystals as Trifunctional Electrocatalysts for Overall Water Splitting Powered by a Zinc–Air Battery, Adv. Mater. 30 (2018) 1705796.

[32] J. Jiang, Q. Liu, C. Zeng, L. Ai, Cobalt/molybdenum carbide@N-doped carbon as a bifunctional electrocatalyst for hydrogen and oxygen evolution reactions, J. Mater. Chem. A. 5 (2017) 16929.

[33] Y.J. Tang, C.H. Liu, W. Huang, X.L. Wang, L.Z. Dong, S.L. Li, Y.Q. Lan, Bimetallic Carbides-Based Nanocomposite as Superior Electrocatalyst for Oxygen Evolution Reaction, ACS Appl. Mater. Interfaces. 9 (2017) 16977.

[34] K. Elumeeva, J. Masa, D. Medina, E. Ventosa, S. Seisel, Y.U. Kayran, A. Genç, T. Bobrowski, P. Weide, J. Arbiol, M. Muhler, W. Schuhmann, Cobalt boride modified with N-doped carbon nanotubes as a high-performance bifunctional oxygen electrocatalyst, J. Mater. Chem. A. 5 (2017) 21122.

[35] N. Xu, G. Cao, Z. Chen, Q. Kang, H. Dai, P. Wang, Cobalt nickel boride as an active electrocatalyst for water splitting, J. Mater. Chem. A. 5 (2017) 12379.

[36] J.M.V. Nsanzimana, Y. Peng, Y.Y. Xu, L. Thia, C. Wang, B.Y. Xia, X. Wang, An Efficient and Earth-Abundant Oxygen-Evolving Electrocatalyst Based on Amorphous Metal Borides, Adv. Energy Mater. 8 (2018) 1701475.

[37] H. Chen, S. Ouyang, M. Zhao, Y. Li, J. Ye, Synergistic Activity of Co and Fe in Amorphous Cox-Fe-B Catalyst for Efficient Oxygen Evolution Reaction, ACS Appl. Mater. Interfaces. 9 (2017) 40333.

[38] H. Sun, J. Meng, L. Jiao, F. Cheng, J. Chen, A review of transition-metal boride/phosphide-based materials for catalytic hydrogen generation from hydrolysis of boron-hydrides, Inorg. Chem. Front. 5 (2018) 760.

[39] P.K. Singh, T. Das, Generation of hydrogen from $NaBH_4$ solution using metal-boride (CoB, FeB, NiB) catalysts, Int. J. Hydrogen Energy. 42 (2017) 29360.

[40] V.I. Simagina, A.M. Ozerova, O. V. Komova, G. V. Odegova, D.G. Kellerman, R. V. Fursenko, E.S. Odintsov, O. V. Netskina, Cobalt boride catalysts for small-scale energy application, Catal. Today. 242 (2015) 221.

[41] V.I. Simagina, O. V. Komova, A.M. Ozerova, O. V. Netskina, G. V. Odegova, D.G. Kellerman, O.A. Bulavchenko, A. V. Ishchenko, Cobalt oxide catalyst for hydrolysis

of sodium borohydride and ammonia borane, Appl. Catal. A Gen. 394 (2011) 86.

[42] J. Masa, P. Weide, D. Peeters, I. Sinev, W. Xia, Z. Sun, C. Somsen, M. Muhler, W. Schuhmann, Amorphous Cobalt Boride (Co_2B) as a Highly Efficient Nonprecious Catalyst for Electrochemical Water Splitting: Oxygen and Hydrogen Evolution, Adv. Energy Mater. 6 (2016) 1502313.

[43] C. Xue, G. Li, J. Wang, Y. Wang, L. Li, Fe^{3+}doped amorphous $Co_2BO_y(OH)_z$ with enhanced activity for oxygen evolution reaction, Electrochim. Acta. 280 (2018) 1.

[44] G. Liu, D. He, R. Yao, Y. Zhao, M. Wang, N. Li, J. Li, Amorphous CoFeBO nanoparticles as highly active electrocatalysts for efficient water oxidation reaction, Int. J. Hydrogen Energy. 43 (2018) 6138.

[45] E.A. Turhan, S.V.K. Nune, E. Ülker, U. Şahin, Y. Dede, F. Karadas, Water Oxidation Electrocatalysis with a Cobalt Borate-Based Hybrid System Under Neutral Conditions, Chem. Eur. J. 24 (2018) 10372.

[46] S. Carenco, D. Portehault, C. Boissière, N. Mézailles, C. Sanchez, Nanoscaled metal borides and phosphides: Recent developments and perspectives, Chem. Rev. 113 (2013) 7981.

[47] S. Zhong, C. Zhan, D. Cao, Zeolitic imidazolate framework-derived nitrogen-doped porous carbons as high performance supercapacitor electrode materials, Carbon 85 (2015) 51.

[48] W. Sun, X. Zhai, L. Zhao, Synthesis of ZIF-8 and ZIF-67 nanocrystals with well-controllable size distribution through reverse microemulsions, Chem. Eng. J. 289 (2016) 59.

[49] K. Zhou, B. Mousavi, Z. Luo, S. Phatanasri, S. Chaemchuen, F. Verpoort, Characterization and properties of Zn/Co zeolitic imidazolate frameworks vs. ZIF-8 and ZIF-67, J. Mater. Chem. A. 5 (2017) 952.

[50] G. Zhong, D. Liu, J. Zhang, The application of ZIF-67 and its derivatives: adsorption, separation, electrochemistry and catalysts, J. Mater. Chem. A. 6 (2018) 1887.

[51] H.X. Zhong, J. Wang, Y.W. Zhang, W.L. Xu, W. Xing, D. Xu, Y.F. Zhang, X.B. Zhang, ZIF-8 derived graphene-based nitrogen-doped porous carbon sheets as highly efficient and durable oxygen reduction electrocatalysts, Angew. Chem. Int. Ed. 53 (2014) 14235.

[52] J. Yang, F. Zhang, H. Lu, X. Hong, H. Jiang, Y. Wu, Y. Li, Hollow Zn/Co ZIF Particles Derived from Core-Shell ZIF-67@ZIF-8 as Selective Catalyst for the Semi-Hydrogenation of Acetylene, Angew. Chem. Int. Ed. 54 (2015) 10889.

[53] Y. Hao, Y. Xu, J. Liu, X. Sun, Nickel-cobalt oxides supported on Co/N decorated graphene as an excellent bifunctional oxygen catalyst, J. Mater. Chem. A. 5 (2017) 5594.

[54] W. Yang, X. Liu, L. Chen, L. Liang, J. Jia, A metal-organic framework devised Co-N doped carbon microsphere/nanofiber hybrid as a free-standing 3D oxygen catalyst, Chem. Commun. 53 (2017) 4034.

[55] Y. Deng, Y. Dong, G. Wang, K. Sun, X. Shi, L. Zheng, X. Li, S. Liao, Well-Defined ZIF-Derived Fe-N Codoped Carbon Nanoframes as Efficient Oxygen Reduction Catalysts, ACS Appl. Mater. Interfaces. 9 (2017) 9699.

[56] X. Yang, J. Chen, J. Hu, S. Zhao, J. Zhao, X. Luo, Metal organic framework-derived

$Zn_{1-x}Co_x$-ZIF@$Zn_{1-x}Co_xO$ hybrid photocatalyst with enhanced photocatalytic activity through synergistic effect, Catal. Sci. Technol. 8 (2018) 573.

[57] Z.F. Huang, J. Song, K. Li, M. Tahir, Y.T. Wang, L. Pan, L. Wang, X. Zhang, J.J. Zou, Hollow Cobalt-Based Bimetallic Sulfide Polyhedra for Efficient All-pH-Value Electrochemical and Photocatalytic Hydrogen Evolution, J. Am. Chem. Soc. 138 (2016) 1359.

[58] J. Zhang, L. Yu, X.W.D. Lou, Embedding CoS_2 nanoparticles in N-doped carbon nanotube hollow frameworks for enhanced lithium storage properties, Nano Res. 10 (2017) 4298.

[59] Z. Chen, M. Liu, R. Wu, Strongly coupling of Co_9S_8/Zn-Co-S heterostructures rooted in carbon nanocages towards efficient oxygen evolution reaction, J. Catal. 361 (2018) 322.

[60] X. Xiao, C.T. He, S. Zhao, J. Li, W. Lin, Z. Yuan, Q. Zhang, S. Wang, L. Dai, D. Yu, A general approach to cobalt-based homobimetallic phosphide ultrathin nanosheets for highly efficient oxygen evolution in alkaline media, Energy Environ. Sci. 10 (2017) 893.

[61] P. He, X. Yu, X. Wen, D. Lou, Carbon-Incorporated Nickel – Cobalt Mixed Metal Phosphide Nanoboxes with Enhanced Electrocatalytic Activity for Oxygen Evolution, Angew. Chem. 129 (2017) 3955.

[62] Y. Pan, K. Sun, S. Liu, X. Cao, K. Wu, W.C. Cheong, Z. Chen, Y. Wang, Y. Li, Y. Liu, D. Wang, Q. Peng, C. Chen, Y. Li, Core-Shell ZIF-8@ZIF-67-Derived CoP Nanoparticle-Embedded N-Doped Carbon Nanotube Hollow Polyhedron for Efficient

Overall Water Splitting, J. Am. Chem. Soc. 140 (2018) 2610.

[63] S. Dou, X. Li, L. Tao, J. Huo, S. Wang, Cobalt nanoparticle-embedded carbon nanotube/porous carbon hybrid derived from MOF-encapsulated Co_3O_4 for oxygen electrocatalysis, Chem. Commun. 52 (2016) 9727.

[64] X. Li, Z. Niu, J. Jiang, L. Ai, Cobalt nanoparticles embedded in porous N-rich carbon as an efficient bifunctional electrocatalyst for water splitting, J. Mater. Chem. A. 4 (2016) 3204.

[65] M. Xu, L. Han, Y. Han, Y. Yu, J. Zhai, S. Dong, Porous CoP concave polyhedron electrocatalysts synthesized from metal-organic frameworks with enhanced electrochemical properties for hydrogen evolution, J. Mater. Chem. A. 3 (2015) 21471.

[66] W. Shuang, L. Kong, M. Zhong, D. Wang, J. Liu, X.-H. Bu, Rational design of Co embedded N,S-codoped carbon nanoplates as anode materials for high performance lithium-ion batteries, Dalton. Trans. 47 (2018) 12385.

[67] Y. Li, S. Niu, D. Rakov, Y. Wang, M. Cabán-Acevedo, S. Zheng, B. Song, P. Xu, Metal organic framework-derived CoPS/N-doped carbon for efficient electrocatalytic hydrogen evolution, Nanoscale. 10 (2018) 7291.

[68] R. Wu, X. Qian, X. Rui, H. Liu, B. Yadian, K. Zhou, J. Wei, Q. Yan, X.-Q. Feng, Y. Long, L. Wang, Y. Huang, Zeolitic Imidazolate Framework 67-Derived High Symmetric Porous Co_3O_4 Hollow Dodecahedra with Highly Enhanced Lithium Storage Capability, Small. 10 (2014) 1932.

[69] J. Yang, H. Liu, W.N. Martens, R.L. Frost, Synthesis and Characterization of Cobalt Hydroxide , Cobalt Oxyhydroxide , and Cobalt Oxide Nanodiscs, J. Phys. Chem. *C*

114 (2010) 111.

[64] S. Liu, Z. Wang, S. Zhou, F. Yu, M. Yu, C.Y. Chiang, W. Zhou, J. Zhao, J. Qiu, Metal–Organic-Framework-Derived Hybrid Carbon Nanocages as a Bifunctional Electrocatalyst for Oxygen Reduction and Evolution, Adv. Mater. 29 (2017) 1700874.

[70] T. Zhu, J.S. Chen, X.W. Lou, Shape-controlled synthesis of porous Co_3O_4 nanostructures for application in supercapacitors, J. Mater. Chem. 20 (2010) 7015.

[71] A. J. Bard and L. R. Faulkner, Electrochemical Methods, Wiley, New York, 2nd edn, 2011.

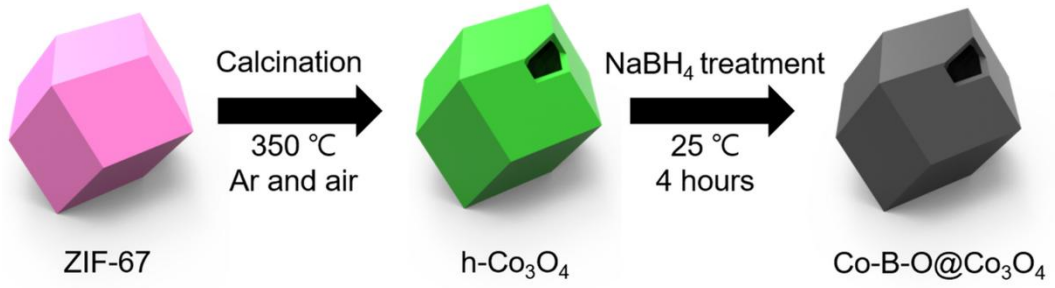

Scheme 1. Schematic illustration of the preparation process of Co-B-O@Co_3O_4.

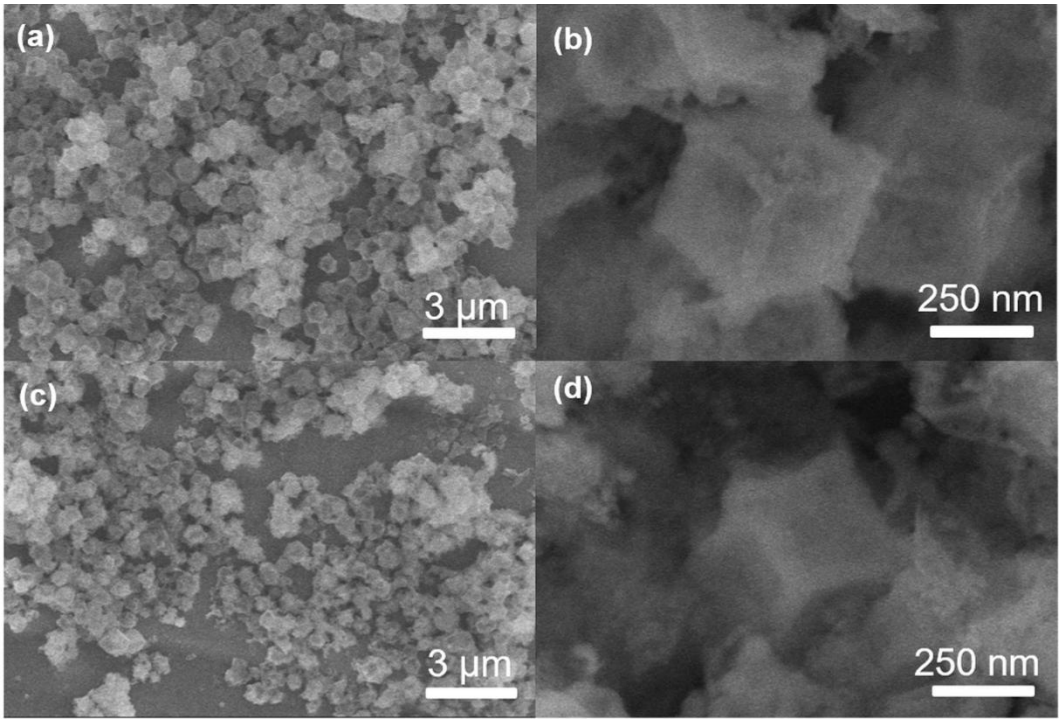

Fig. 1. SEM images of h-Co_3O_4 (a, b) and Co-B-O@Co_3O_4 (c, d).

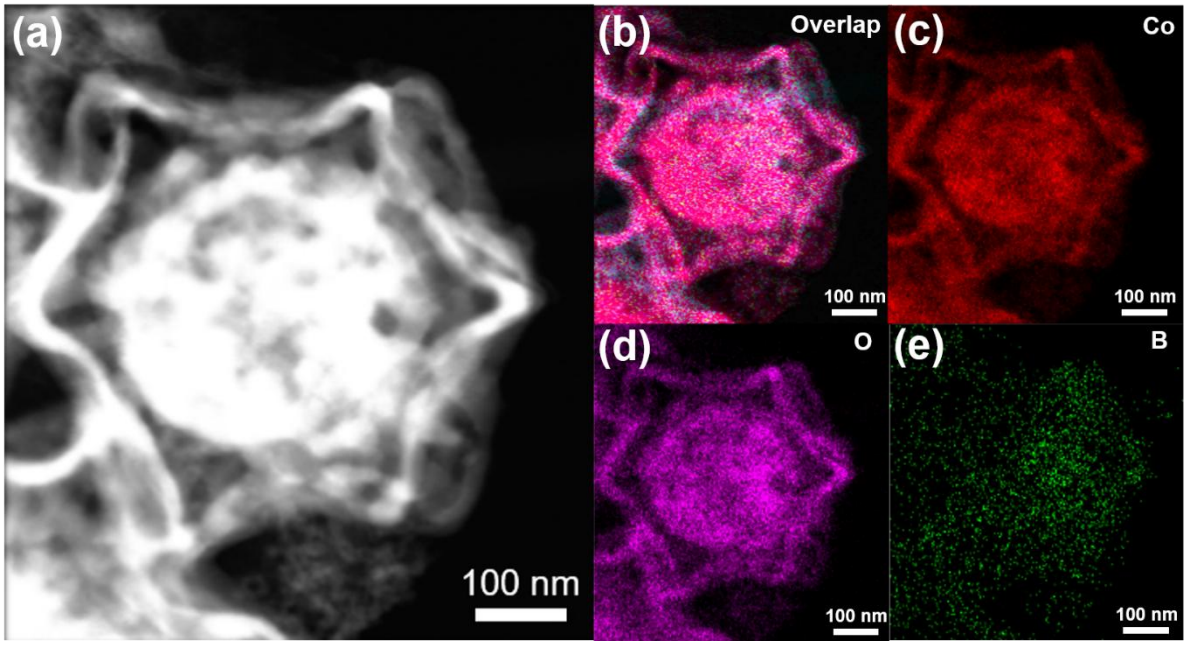

Fig. 2. TEM image of Co-B-O@Co_3O_4 catalyst (a). An EDS mapping image of Co-B-O@Co_3O_4 catalyst (b) and analyzed atom; Co (c), O (d) and B (e).

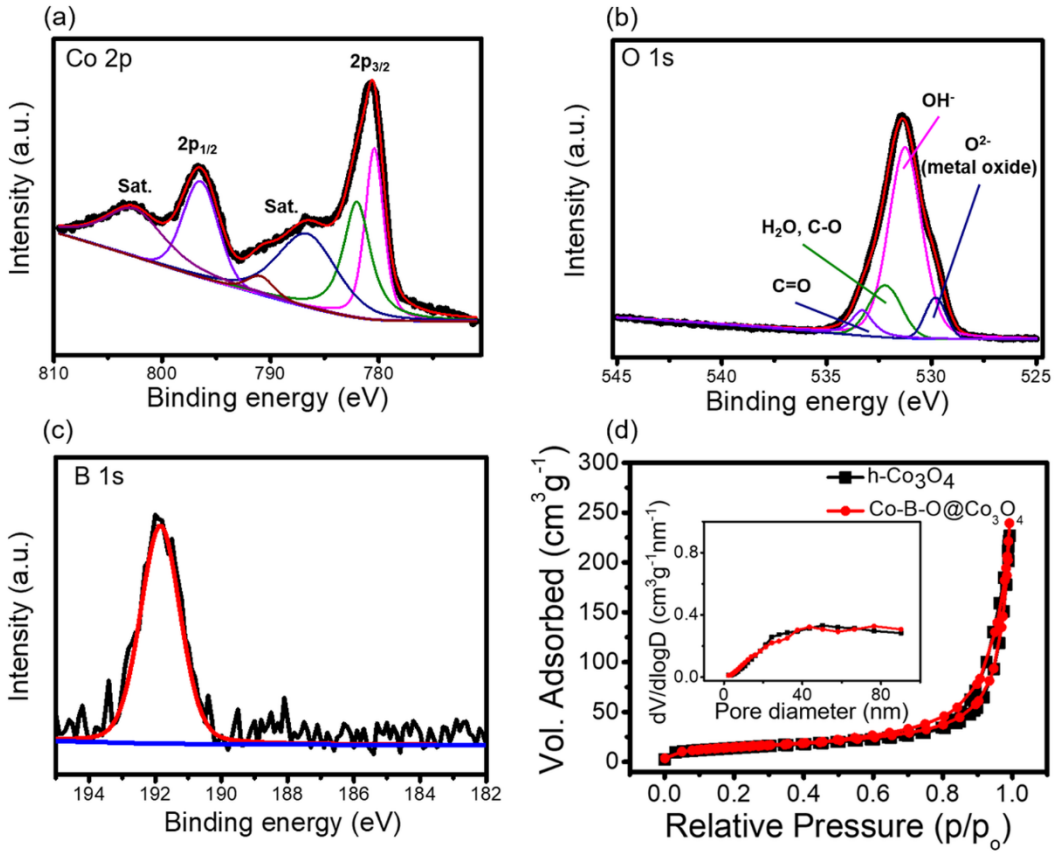

Fig. 3. XPS analysis of h-Co_3O_4 and Co-B-O@Co_3O_4 catalyst; Co 2p (a), O 1s (b), and B 1s (c). BET analysis of h-Co_3O_4 and Co-B-O@Co_3O_4 catalyst (d). Inset; pore distribution diagram of h-Co_3O_4 and Co-B-O@Co_3O_4.

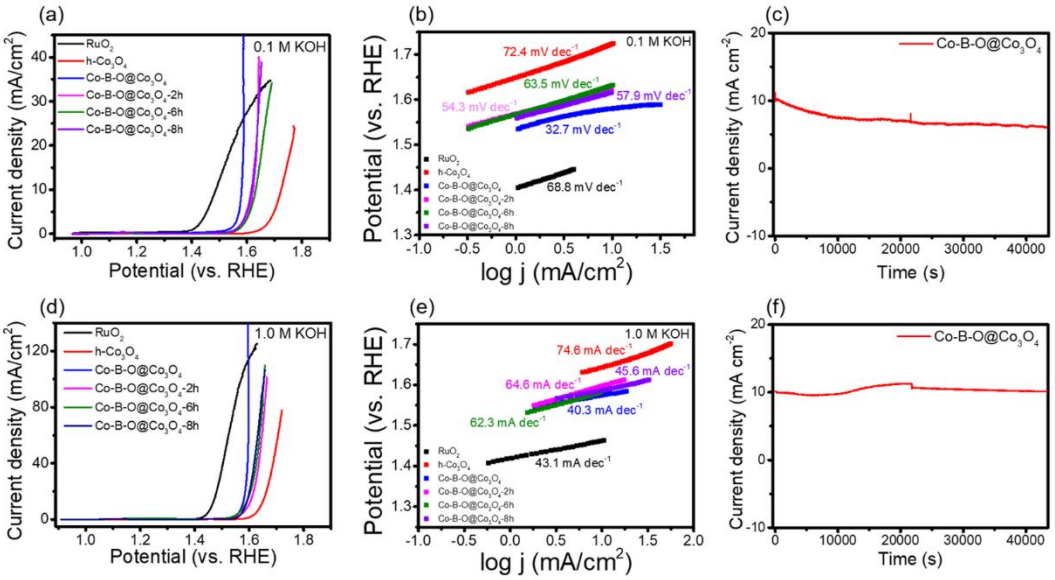

Fig. 4. LSV (a, d) and Tafel curves (b, e) of Co-B-O@Co_3O_4 and compared catalysts in 0.1 M and 1.0 M KOH with the scan rate of 5 mVs^{-1} at room temperature. A stability test (c, f) result of Co-B-O@Co_3O_4 catalyst to maintain 10 mA cm^{-2} for 12 h in 0.1 M and 1.0 M KOH, respectively.

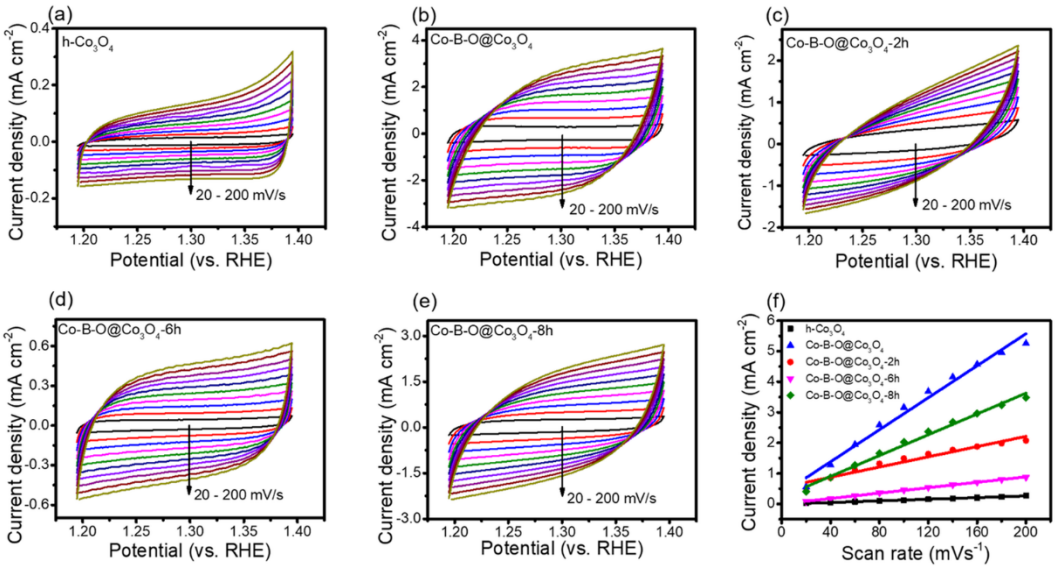

Fig. 5. Double-layer capacitance (C_{dl}) study of h-Co_3O_4 (a), Co-B-O@Co_3O_4 (b), Co-B-O@Co_3O_4-2h (c), Co-B-O@Co_3O_4-6h (d) and Co-B-O@Co_3O_4-8h (e) in 0.1 M KOH with the potential range between 1.20 and 1.40 V (scan rate; 20 - 200 mV s^{-1}). Linear plot (f) of scan rate vs. current density according to the data from the C_{dl} data. The C_{dl} was calculated as follows: $C_{dl} = \Delta j / \upsilon$, $\Delta j = j_a - j_c$: Charging current (mA cm^{-2}), aka. 'slope', υ : scan rate (mVs^{-1}).